Critical-point screening in random wave fields

Isaac Freund

Jack and Pearl Resnick Advanced Technology Institute and Department of Physics, Bar-Ilan University, Ramat-Gan 52900, Israel

Michael Wilkinson

Department of Physics and Applied Physics, John Anderson Building, University of Strathclyde, Glasgow, G4 0NG, UK

Received April 7, 1998; accepted July 6, 1998

Screening of vortices and other critical points in a two-dimensional random Gaussian field is studied by using large-scale computer simulations and analytic theory. It is shown that the topological charge imbalance and its variance in a bounded region can be obtained from signed zero crossings on the boundary of the region. A first-principles Gaussian theory of these zero crossings and their correlations is derived for the vortices and shown to be in good agreement with the computer simulation. An exact relationship is obtained between the variance of the charge imbalance and the charge correlation function, and this relationship is verified by comparison with the data. The results obtained are extended to arbitrarily shaped volumes in isotropic spaces of higher dimension. © 1998 Optical Society of America [S0740-3232(98)00711-X]

OCIS codes: 030.6140, 030.6600, 290.5880.

1. INTRODUCTION

Screening is of far-reaching importance in such diverse areas as atomic, solid-state, and plasma physics, as well as in electrochemistry, chemical thermodynamics, reaction kinetics, etc. Here we show that screening is also of special importance in random optical fields. In these fields the relevant charges are topological rather than electrostatic, and we find that critical points with topological charges (indices) of opposite sign display a strong tendency to screen one another. As a result, minima are surrounded by clouds of maxima, maxima and minima are surrounded by clouds of saddle points, positive vortices are surrounded by negative vortices, etc. We find that even in highly random Gaussian fields, screening is substantially complete within a single coherence area, and that screening in these fields is so pervasive that stationary points of the imaginary part of the wave function screen those of the real part of the wave function, a seemingly paradoxical result, since these two components of the field are known to be statistically independent. We note that an important consequence of screening is that it strongly damps out all charge fluctuations, radically altering the charge imbalance within a bounded region.[1]

In Section 2 we show with the aid of simple topological theorems that the charge imbalance and its variance may be easily determined from measurements made only on the boundary of the region. We provide data for the vortices and for the stationary points of the real part of the wave function and of the intensity. We also compare the data for the vortices with a first-principles calculation based on Gaussian statistics. In Section 3 we present data for the charge correlation functions of a number of different critical points, discuss the influence of screening, and compare our results for the vortices with a first-principles calculation that is due to Halperin.[2] In Section 4 we develop an exact relationship between the charge correlation function and the variance of the charge imbalance in a bounded region and illustrate this relationship quantitatively by using our data for the vortices. We also extend our results to arbitrary volumes in isotropic spaces of higher dimension. In Section 5 we briefly summarize our main findings. Although we concentrate on the critical points of a Gaussian random field, screening is not restricted to these fields, and the results found here may prove useful in such diverse areas as the Kosterliz–Thouless transition in liquid helium[3] and Chern numbers in the quantum Hall effect.[4,5]

To avoid a confusing proliferation of symbols, in what follows we consistently employ the following scheme. If the value of some quantity for a particular realization is denoted by (say) Q, we will denote the corresponding ensemble average by $\langle Q\rangle$ and the corresponding (say) two-dimensional spatial density by $Q(\mathbf{r})$. Then $Q(\mathbf{r}_i)\mathrm{d}x\mathrm{d}y$ is the contribution to Q of an element of area $\mathrm{d}x\mathrm{d}y$ centered at $\mathbf{r}=\mathbf{r}_i$, and $Q=\int\int \mathrm{d}x\mathrm{d}y\ Q(\mathbf{r})$, where the integration is over the appropriate region of the realization. If Q corresponds to a quantity measured along a line rather than over an area, then in anisotropic media the direction of measurement needs to be specified as being parallel to either the x or the y axis. In these cases we use either Q_x, Q_y or $Q^{(x)}$, $Q^{(y)}$ to indicate the corresponding directions.

2. TOPOLOGICAL CHARGES IN A BOUNDED REGION

A. Vortices

The generic topological singularities in the two-dimensional isotropic fields of interest here are the vortices.[6–8] These are isolated first-order zeros at which the amplitude α vanishes and the phase ϕ becomes singu-

lar (undefined). Writing the optical field $\Psi(x, y) = \alpha \exp(i\phi) = R(x, y) + iI(x, y)$, where $R(I)$ is the real (imaginary) part of the wave function, yields

$$\phi = \arctan(I/R), \tag{1}$$

and $\alpha = 0$ implies that $R = I = 0$ at vortex centers. Accordingly, vortices are always found at intersections of the zero crossings Z_R and Z_I of R and I, and in the generic fields of interest here the converse is also true and every intersection of Z_R and Z_I houses a vortex. As vortices are first-order zeros, in their immediate vicinity R and I may be expanded as $R(x, y) = R_x^0 x + R_y^0 y$, $I(x, y) = I_x^0 x + I_y^0 y$, where $R_x^0 = (\partial R/\partial x)_{x=y=0}$, etc., and where we have shifted the origin to the vortex center. Taking as the simplest example $R_x^0 = 1$, $R_y^0 = I_x^0 = 0$, $I_y^0 = \pm 1$, we have $\Psi_\pm = x \pm iy = r \exp(\pm i\theta)$, so that vortices may be either positive or negative depending on the direction of circulation of the phase $\phi = \pm\theta$. The sign (± 1) of a vortex is often referred to as its topological charge, since under continuous evolution of the wave function this quantity is conserved. (Mathematicians use the term winding number because the phase winds by integer multiples of 2π in one circuit.)

Writing the total number of vortices within some bounded region as $N = N_+ + N_-$, where $N_\pm$ is the number of positive/negative vortices, the net charge $\Delta N = N_+ - N_-$ may be found either by directly measuring N_+ and N_- or, possibly more conveniently, by measuring ϕ as one walks (counterclockwise) along the boundary. Denoting the starting point of the walk by 1 and its end point by 2, after one complete circuit we have

$$\Delta N = \frac{1}{2\pi}(\phi_2 - \phi_1). \tag{2}$$

In Gaussian and other charge-neutral fields, $\langle \Delta N \rangle = 0$, where $\langle \cdot \rangle$ implies an ensemble average, and charge fluctuations are characterized in lowest nonzero order by the variance $\langle (\Delta N)^2 \rangle$. In measuring this quantity, we make use of Eq. (2), as this avoids the difficult task of explicitly locating, characterizing, and counting all vortices within the region of interest.

B. Stationary Points

Associated with each stationary point of a continuous function f, such as R, I, or the intensity $U = \alpha^2 = R^2 + I^2$, is the topological (Poincaré) index, a signed integer that is $+1$ for extrema (maxima and minima) and -1 for saddle points.[9,10] These integers may also be considered as topological charges, since they are conserved under continuous evolution of the wave function, with the net charge (index) within some bounded region being the sum of the indices of the stationary points contained within the region. For these charges we can obtain the equivalents of Eqs. (1) and (2) by making an exact mapping of the stationary points of f onto the vortices of ϕ.

We start by noting that the stationary points of f are always located at intersections of the zero crossings Z_x of $f_x = \partial f/\partial x$ and Z_y of $f_y = \partial f/\partial y$. Forming the vector field $\nabla f = f_x \hat{x} + f_y \hat{y}$, where $\hat{x}$ and $\hat{y}$ are unit vectors along x and y, respectively, we have the following for the angle Θ that the vectors make with the x axis:

$$\Theta = \arctan(f_y/f_x). \tag{3}$$

The two-component vector field ∇f may thus be seen to be completely analogous to the two-component complex optical field Ψ, with f_y replacing I and f_x replacing R. This extends to the singularities of these fields. For the phase field ϕ the topological charge q_v of a singularity (vortex) is given by

$$q_v = \mathrm{sgn}(R_x I_y - R_y I_x), \tag{4}$$

and for the singularities of the equivalent field Θ (the stationary points of f), the charge q_s is given by

$$q_s = \mathrm{sgn}(f_{xx} f_{yy} - f_{xy} f_{yx}), \tag{5}$$

with $f_{yx} = f_{xy}$. In addition, just as the vortices of the phase field ϕ are constrained to alternate in sign along every Z_R and Z_I,[11,12] the stationary points of f are constrained to alternate in sign (index) along every Z_x and Z_y.[13–15] Thus f extrema are positive Θ vortices and f saddles are negative Θ vortices, and using the equivalent of Eq. (2),

$$\Delta N = \frac{1}{2\pi}(\Theta_2 - \Theta_1), \tag{6}$$

we may find the net charge within some bounded region by measuring Θ along the boundary. In computing ΔN by using Eq. (6), we take Θ to be a continuous function of arc length (i.e., not folded back into the interval 0–2π).

We have used the above mapping to obtain Eq. (6), since it provides considerable insight into the close relationship between vortices and other critical points. This same result, however, may be obtained directly from the properties of the index by recalling that the net index of all critical points within a bounded region can be found from a contour map by measuring the directions $\mathrm{d}y/\mathrm{d}x$ of contour lines that cross the boundary.[9,10] Writing $\mathrm{d}y/\mathrm{d}x = -f_x/f_y = \tan(\Theta - \pi/2)$, we recover Eq. (3) and hence Eq. (6).

In summary, then, we can assign a series of topological charges to the critical points of the various fields of interest here and use Eqs. (3) and (6) to obtain ΔN for critical points of the phase ϕ, the real part R of the wave function, and the intensity U by making the following identifications: (1) For the phase we form two distinct sets of critical points. The first consists only of positive/negative vortices with charges $+1/-1$, and for this set we have $f_x = R$, $f_y = I$. The second set consists of the combined critical points: vortices, extrema, and saddles. For this set vortices and extrema have a charge of $+1$, saddles have a charge of -1, and $f_x = \phi_x$, $f_y = \phi_y$.[16] (2) For the real (imaginary) parts of the wave function, extrema have a charge of $+1$, saddles have a charge of -1, and $f_x = R_x$ (I_x), $f_y = R_y$ (I_y). (3) For the intensity, extrema have a charge of $+1$, saddles have a charge of -1, and $f_x = U_x$, $f_y = U_y$. Below we use these results to obtain explicit expressions for $\langle (\Delta N)^2 \rangle$ for the different fields.

C. Boundary Walk

There exists a shortcut in the application of Eq. (6) that is convenient for both experimental measurement and theo-

retical calculation. From Eq. (3) it follows that at zero crossings of f_y, $\Theta = m\pi$, and at zero crossings of f_x, $\Theta = (m + 1/2)\pi$, where m is a positive/negative integer. Accordingly, it suffices simply to count the numbers n_+ (n_-) of up (down) crossings of Θ at the zero crossings of either f_x or f_y, where a given zero crossing is an up (down) crossing of Θ if $\sigma = \mathrm{sgn}(\partial\Theta/\partial s)$ is positive (negative), with s a unit of length along the path. From Eq. (3) it follows that for a path segment that parallels the x axis (y axis) along which $\sigma = \sigma_x$ ($\sigma = \sigma_y$), we have

$$\sigma_x(f_y) = \mathrm{sgn}(f_x f_{xy}), \qquad \sigma_x(f_x) = \mathrm{sgn}(-f_y f_{xx}), \quad (7a)$$

$$\sigma_y(f_y) = \mathrm{sgn}(f_x f_{yy}), \qquad \sigma_y(f_x) = \mathrm{sgn}(-f_y f_{xy}), \quad (7b)$$

where the function whose zero crossings are counted is shown explicitly as the argument of σ. Then

$$\Delta N = \frac{1}{2}\Delta n, \quad (8)$$

with $\Delta n = n_+ - n_-$, and, from Eq. (8),

$$\langle(\Delta N)^2\rangle = \tfrac{1}{4}[\langle(\Delta n^{(x)})^2\rangle + \langle(\Delta n^{(y)})^2\rangle]. \quad (9)$$

Here $\Delta n^{(x)} = n_+^{(x)} - n_-^{(x)}$, $\Delta n^{(y)} = n_+^{(y)} - n_-^{(y)}$, and $n_{+/-}^{(x)}$ ($n_{+/-}^{(y)}$) are the number of up/down crossings counted along the x axis (y axis). For reasons that will soon become apparent, in writing Eq. (9) we have set $\langle\Delta n^{(x)}\Delta n^{(y)}\rangle = 0$.

Viewing our boundary walk as a possibly correlated random walk in which each zero crossing of f_x or f_y contributes either $+1$ or -1 to Δn and neglecting end corrections, we write

$$\langle(\Delta n^{(x)})^2\rangle = \gamma_x\langle n^{(x)}\rangle, \quad (10a)$$

$$\langle(\Delta n^{(y)})^2\rangle = \gamma_y\langle n^{(y)}\rangle, \quad (10b)$$

where $n^{(x)} = n_+^{(x)} + n_-^{(x)}$, $n^{(y)} = n_+^{(y)} + n_-^{(y)}$, and γ_x (γ_y) measures the average degree of correlation between zero crossings on the x-axis (y-axis) segments. For no correlation we have $\gamma = 1$, and for bunching (antibunching)[17] we have $\gamma > 1$ ($0 < \gamma < 1$). Choosing our bounded region to be a rectangular box of side L_x along the x axis and side L_y along the y axis, we have

$$\langle n^{(x)}\rangle = 2n_0^{(x)}L_x, \quad (11a)$$

$$\langle n^{(y)}\rangle = 2n_0^{(y)}L_y, \quad (11b)$$

where $n_0^{(x)}$ ($n_0^{(y)}$) is the average lineal number density of zero crossings of f_x or f_y along the x axis (y axis). From Eqs. (9)–(11) we then have the following for one complete circuit:

$$\langle(\Delta N)^2\rangle = \frac{1}{2}[\gamma_x n_0^{(x)}L_x + \gamma_y n_0^{(y)}L_y]. \quad (12)$$

Now the fields ϕ, R, I, and U are all statistically stationary and isotropic, so that $\langle(\Delta N)^2\rangle$ must be invariant under (say) a 90° rotation of our box. This permits us to write $\gamma_x n_0^{(x)}L_x + \gamma_y n_0^{(y)}L_y = \gamma_x n_0^{(x)}L_y + \gamma_y n_0^{(y)}L_x$, and since L_x and L_y may be chosen arbitrarily and independently, this implies that

$$\gamma_x n_0^{(x)} = \gamma_y n_0^{(y)}. \quad (13)$$

We emphasize that both $\gamma_i = \gamma_i(f_j)$ and $n_0^{(i)} = n_0^{(i)}(f_j)$ are measured along the same direction ($i = x$ or y) for the same function f_j ($j = x$ or y). Since $\langle(\Delta N)^2\rangle$ cannot, of course, depend on the choice of i and j, we have the obvious symmetry relationships: $\gamma_x(f_x)n_0^{(x)}(f_x) = \gamma_x(f_y)n_0^{(x)}(f_y) = \gamma_y(f_x)n_0^{(y)}(f_x) = \gamma_y(f_y)n_0^{(y)}(f_y)$. Since the parent field is isotropic, invariance under interchange of x and y also yields $n_0^{(x)}(f_y) = n_0^{(y)}(f_x)$ and $\gamma_x(f_y) = \gamma_y(f_x)$. R and I may be interchanged by passing the wave through a 90° phase shifter (uniform glass plate). Since this history cannot be determined from measurements made on the wave field alone, invariance under interchange of R and I yields for the vortices, for example, $\gamma_x(R) = \gamma_y(R) = \gamma_x(I) = \gamma_y(I)$ and $n_0^{(x)}(R) = n_0^{(y)}(R) = n_0^{(x)}(I) = n_0^{(y)}(I)$. For simplicity, in what follows we write $\gamma_i(f_j)n_0^{(i)}(f_j) = \gamma n_0$ when there is no chance for confusion. Defining $P = 2(L_x + L_y)$ as the perimeter of the box, we obtain our final result:

$$\langle(\Delta N)^2\rangle = \tfrac{1}{4}\gamma n_0 P. \quad (14)$$

As shown below by both experiment and theory, for all the fields studied here correlations between zero crossings are short ranged, falling to zero on length scales that are always of the order of the transverse coherence length L_{coh} of the field. This implies that for boxes large compared with a coherence area different sides of the box are uncoupled, which provides the justification for our setting $\langle\Delta n^{(x)}\Delta n^{(y)}\rangle = 0$ in Eq. (9). But this also implies that the segments L_x and L_y need not be part of the same box! And this, in turn, implies that $\langle(\Delta N)^2\rangle$ for a given field can be measured or calculated simply by counting up and down crossings along a *straight* line of length P that parallels (say) the x axis. This possibly unexpected conclusion is verified by the data given below. Worth noting is that although Eq. (14) is obtained here explicitly for a rectangular box, in Section 4 it becomes apparent that this form remains true also for a boundary of arbitrary shape, provided only that all fingers and fjords have widths and radii of curvature large compared with L_{coh}.

D. Measurements of the Variance $\langle(\Delta N)^2\rangle$

In curve a of Fig. 1 we plot $\langle(\Delta N)^2\rangle$ versus P for the vortices. These data were obtained by extending recent large-scale computer simulations of an isotropic Gaussian wave field.[18,19] In this simulation the field–field autocorrelator $W(\Delta r)$ is the besinc function $2J_1(\alpha\Delta r)/(\alpha\Delta r)$, where J_1 is a Bessel function of integer order 1 and $\alpha = 0.2$ is a constant set by the numerical parameters of the simulation. This form for the field autocorrelator corresponds to scattering of coherent laser light from a uniformly illuminated, highly random circular sample.[20] We denote the unit of length employed in the simulation by a pixel, so that the transverse coherence length, which is conventionally taken as the distance $j_{1,1}$ to the first zero of J_1, is $L_{\mathrm{coh}} = 19.16$ pixels.

Each point in Fig. 1 is an average over 1010 independent realizations, with each realization being constructed from 10,000 randomly phased Fourier components. Ten of the realizations served as controls for which ΔN was determined both by direct count and by a boundary walk using the methods of Subsection 2.C, with perfect agree-

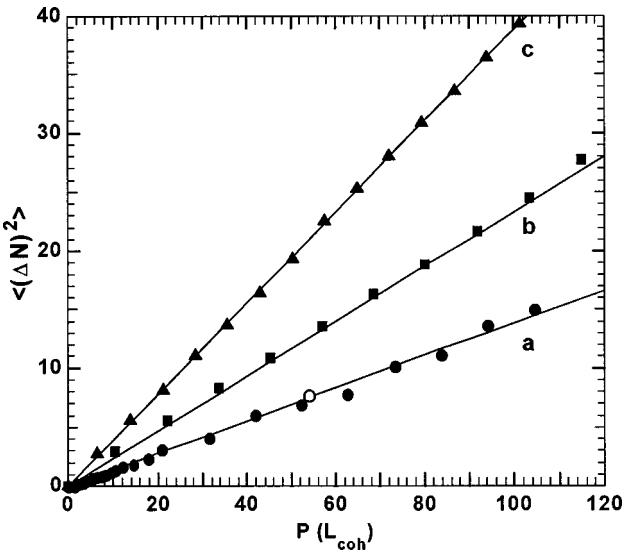

Fig. 1. Variance $\langle(\Delta N)^2\rangle$ of the topological charge imbalance: curve a, vortices; curve b, stationary points of the real part of the wave function; curve c, stationary points of the intensity. In curve a the filled circles are for a square box with perimeter P, and the open circle is for a line of length P. All data points in curves b and c are for lines of length P. For all curves P is measured in units of the transverse coherence L_{coh}. The data in curve b are multiplied by 1.5 to prevent overlap with those of curve a. For each data set the line is Eq. (14) with parameters listed in Subsection 2.D.

ment found in all cases between the two methods. For the 24 data points shown as filled circles, ΔN was obtained from a walk along the perimeter P of a square box, and for the open circle at $P = 53.9L_{\mathrm{coh}}$ the walk was along a line of length P that paralleled the x axis. Both paths may be seen to yield equivalent results, in accord with the discussion of Subsection 2.C.

The line that passes through the data points of curve a is calculated from Eq. (14) by using $\gamma = 0.9088$, as obtained from two seemingly different first-principles calculations described below. The lineal number density of zero crossings of the real part of the wave function required in Eq. (14) has been given recently for our simulation as $n_0(R) = (10\pi)^{-1} = 0.0318/\mathrm{pixel}$.[21] Since there are no adjustable parameters, these data serve to verify the theory of Subsection 2.C. The region of small P (i.e., small box sizes) for which Eq. (14) no longer holds and for which the data systematically fall below the line is discussed in Section 4.

In curve b of Fig. 1, we plot $\langle(\Delta N)^2\rangle$ versus P as measured for the stationary points of R. For display purposes we have multiplied this data set by a factor of 1.5 to improve visibility, since the points otherwise tend to overlap those in curve a. The (unmodified) data for the stationary points of the intensity U are displayed in curve c. All the data for R and U were obtained by using a linear path of length P, and as above, the lines passing through the data points are calculated from Eq. (14). For curve b, the data for the stationary points of R are $n_0^{(x)}(R_x) = \sqrt{2}/(10\pi) = 0.0450/\mathrm{pixel}$ (Ref. 21) and $\gamma_x(R_x) = 0.72$, as obtained from direct measurement of the zero-crossing charge correlation function described in Subsection 2.F. Corresponding data for the stationary points of U in curve c are $n_0^{(x)}(U_x) = 0.0724/\mathrm{pixel}$ (Ref. 21) and $\gamma_x(U_x) = 1.12$. Values of γ for other combinations of x and y may be obtained from the symmetry relations listed in Subsection 2.C together with the corresponding values for n_0 given in Ref. 21.

Finally, for the combined critical points of phase—vortices, extrema, and saddles—we have limited data obtained by direct count from ten independent realizations, each with $P = 54.3L_{\mathrm{coh}}$. For these data $\langle(\Delta N)^2\rangle = 8.2 \pm 2.7$, which, together with $n_0^{(x)}(\phi_x) = (10\pi)^{-1} = 0.0318/\mathrm{pixel}$,[21] yields $\gamma = 1.0 \pm 0.3$.

E. Probability Density Function of $\langle(\Delta N)^2\rangle$

The random-walk theory of Subsection 2.D implies that for a given value of P the probability density function of ΔN, $\Pi(\Delta N)$, ought to approach asymptotically a Gaussian with variance $\langle(\Delta N)^2\rangle$. To test this for the large range of P shown in Fig. 1, we define $\delta N = \Delta N/\sqrt{P}$, where $\langle(\delta N)^2\rangle = \frac{1}{4}\gamma n_0$, and write

$$\Pi(\delta N) = \frac{1}{[2\pi\langle(\delta N)^2\rangle]^{1/2}} \exp\{-(\delta N)^2/[2\langle(\delta N)^2\rangle]\}. \tag{15}$$

In Fig. 2 we compare Eq. (15) with vortex data for the 25 different values of P in curve a of Fig. 1. Plotted here versus δN are the 25 individual histograms for ΔN, each multiplied by the corresponding value of $\sqrt{P}$ to preserve normalization. As may be seen, all histograms cluster about a single curve that is well described by Eq. (15). (The apparent pileup of data points at $\delta N = 0$ is an artifact that is due to the finite bin size of the parent ΔN histograms, together with the fact that $0/\sqrt{P} \equiv 0$ for all P.) Equally good or better agreement between measurement and calculation is also obtained for R and U (these data are not shown), and since in all cases there are no adjustable parameters, this agreement adds additional support for the theory of Subsection 2.D.

F. Zero-Crossing Charge Correlation Functions

Writing $n_{+/-}(x)\mathrm{d}x$ for the number of positive/negative (up/down) zero crossings between x and $x + \mathrm{d}x$, we have from Eq. (8) that

$$\Delta N = \frac{1}{2}\int_0^P \mathrm{d}x[n_+(x) - n_-(x)], \tag{16}$$

where, as in Subsection 2.D, we take the path to be a line of length P parallel to the x axis. Using $\langle n_+{}^2\rangle = \langle n_-{}^2\rangle$, $\langle n_+(x)n_+(x')\rangle = \langle n_-(x)n_-(x')\rangle$, $\langle n_+(x)n_-(x')\rangle = \langle n_-(x)n_+(x')\rangle$, etc., and defining $\Delta n(x) = n_+(x) - n_-(x)$, we obtain

$$\langle(\Delta N)^2\rangle = \frac{1}{2}\int_0^P \mathrm{d}x \int_0^P \mathrm{d}x'\langle n_+(x)\Delta n(x')\rangle. \tag{17}$$

Defining $u_P(w) = 1$ if $0 \leq w \leq P$ and $u_P(w) = 0$ otherwise, we rewrite Eq. (17) as

$$\langle(\Delta N)^2\rangle = \frac{1}{2}\int_{-\infty}^{\infty} \mathrm{d}x \int_{-\infty}^{\infty} \mathrm{d}x'\; u_P(x)u_P(x')\langle n_+(x)\Delta n(x')\rangle. \tag{18}$$

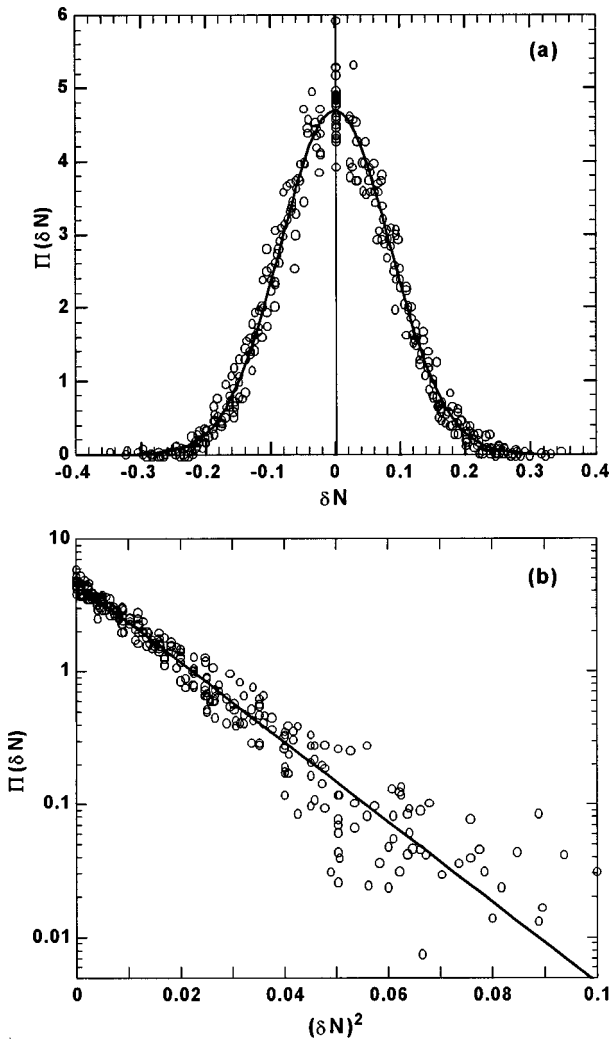

Fig. 2. Probability density function $\Pi(\delta N)$ for the vortices, where $\delta N = \Delta N/\sqrt{P}$. The curves are calculated from Eq. (15).

Changing variables by using $x' = x + \Delta x$, assuming a stationary process for which $\langle n_+(x)\Delta n(x + \Delta x)\rangle = \langle n_+(0)\Delta n(\Delta x)\rangle$, and noting that

$$\int_{-\infty}^{\infty} \mathrm{d}x\; u_P(x)u_P(x + \Delta x) = (P - |\Delta x|)H(P - |\Delta x|), \tag{19}$$

where the Heaviside step function $H(v) = 1$ if $v \geqslant 0$ and vanishes otherwise, yield

$$\langle(\Delta N)^2\rangle = \frac{1}{2}\int_{-P}^{P} \mathrm{d}(\Delta x)(P - |\Delta x|)\langle n_+(0)\Delta n(\Delta x)\rangle. \tag{20}$$

Defining the signed zero-crossing charge correlation function $\Gamma(\Delta x)$ by

$$\langle n_+(0)\Delta n(\Delta x)\rangle = \tfrac{1}{2}n_0[\delta(\Delta x) + \Gamma(\Delta x)], \tag{21}$$

where the factor of 1/2 arises from $\langle n_+\rangle = \frac{1}{2}n_0$ and the Dirac delta function $\delta(\Delta x)$ takes explicit account of the fact that the charge at the origin is always perfectly correlated with itself, we obtain

$$\langle(\Delta N)^2\rangle = \frac{1}{4}n_0P\left[1 + \int_{-P}^{P}\mathrm{d}(\Delta x)\Gamma(\Delta x)\right] - \frac{1}{4}n_0\int_{-P}^{P}\mathrm{d}(\Delta x)|\Delta x|\Gamma(\Delta x). \tag{22}$$

If $\Gamma(\Delta x)$ is short ranged, as is indeed the case, then, for large boxes, only the term in Eq. (22) proportional to P is important, and in the limit $P \to \infty$ we recover Eq. (14) with

$$\gamma = 1 + 2\int_0^{\infty}\mathrm{d}(\Delta x)\Gamma(\Delta x). \tag{23}$$

In Fig. 3 we display $\Gamma(\Delta x/L_{\mathrm{coh}})$ as measured from our simulation for the signed zero crossings of (a) R, (b) R_x, and (c) U_x. As may be seen, in all cases the range of $\Gamma(\Delta x)$ is of the order of the coherence length L_{coh}. For the zero crossings of both R and R_x, $\Gamma(\Delta x)$ is mostly negative, so that adjacent crossings are *anti*correlated in sign, whereas for U_x the correlation is mostly positive. Using the data in Figs. 3(b) and 3(c) to carry out numerically the integration in Eq. (23), we obtain the values for $\gamma_x(R_x)$ and $\gamma_x(U_x)$ listed in Subsection 2.D for the stationary points of R and U. For the vortices $\gamma_x(R)$ is obtained from numerical integration of the solid curve in Fig. 3(a), which is calculated in Subsection 2.G.

G. Gaussian Theory of $\Gamma(\Delta x)$ for the Zero Crossings of R

Returning to Eq. (21), we have

$$\Gamma(x_2 - x_1) = \frac{2}{n_0}\langle n_+(x_1)\Delta n(x_2)\rangle, \tag{24}$$

where the subscripts 1 and 2 now denote two *different* arbitrary positions on the x axis. For calculations involving Gaussian statistics, the operators $\hat{n}_\pm$ corresponding to the individual densities $n_\pm(x)$ may conveniently be written as

$$\hat{n}_\pm = \delta(R_i)|R_i'|H(\mp I_iR_i'), \tag{25}$$

where the subscript i implies evaluating the indicated quantity at the point x_i and $R' = \partial R/\partial x$. As derivations of similar operators have already been given by several authors, we do not derive Eq. (25) but refer the interested reader to the original literature.[2,8,22–24]

For isotropic Gaussian fields the probability density function needed for calculating the expectation value in Eq. (24) may, after implementation of the delta function in Eq. (25), be written as

$$\Pi(I_1, I_2; R_1', R_2') = \Pi_I(I_1, I_2)\Pi_R(R_1', R_2'), \tag{26}$$

where

$$\Pi_I = K_I \exp\{-[a(I_1^2 + I_2^2) + bI_1I_2]\}, \tag{27a}$$

$$\Pi_R = K_R \exp\{-[c(R_1'^2 + R_2'^2) + dR_1'R_2']\}. \tag{27b}$$

As is always the case for Gaussian statistics, all statistical parameters appearing in these probability density functions may be obtained from the autocorrelation function of the field $W(\Delta x)$, and we have

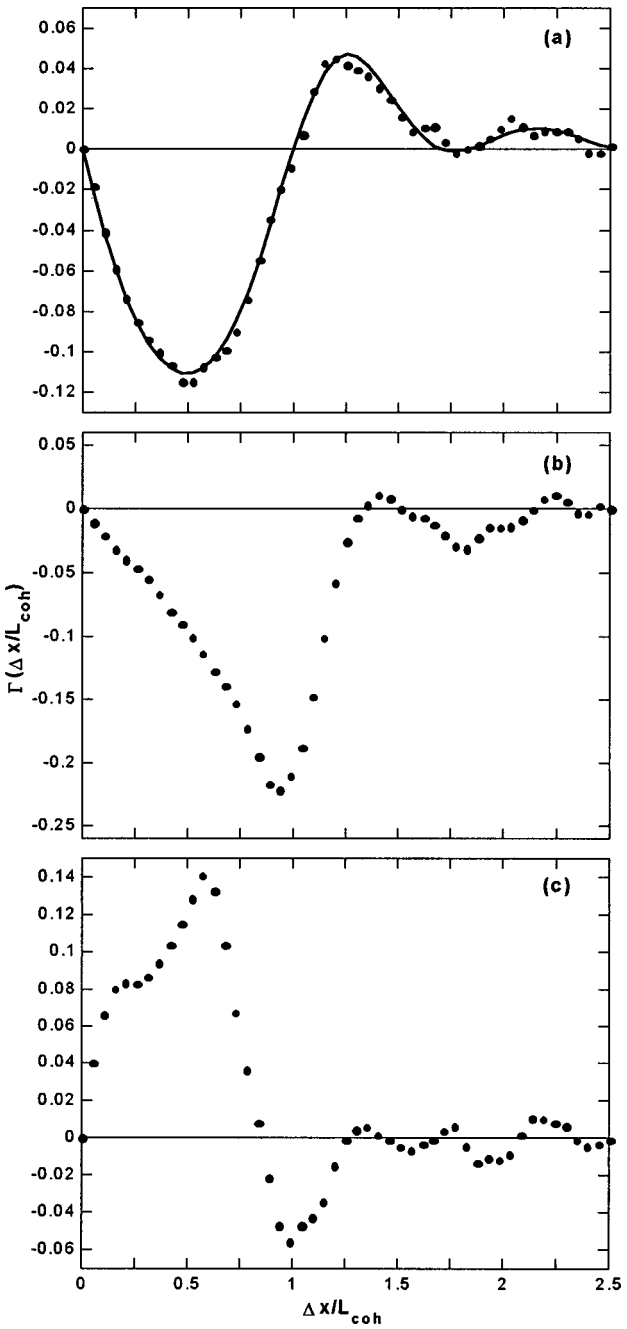

Fig. 3. Zero-crossing charge correlation function $\Gamma(\Delta x/L_{\mathrm{coh}})$ defined in Eq. (21) for (a) the vortices, (b) the real part of the wave function, and (c) the intensity. The curve in (a) is calculated from Eq. (29).

$$
\begin{aligned}
&K_I = (2\pi)^{-1} {D_I}^{-1/2}, \qquad K_R = (2\pi)^{-2} {D_R}^{-1/2},\\
&D_I = 1 - B^2,\\
&D_R = (BE - BF + D^2 + E - F)\\
&\qquad \times (-BE - BF + D^2 + E + F),\\
&a = (2D_I)^{-1}, \qquad b = -BD_I{}^{-1},\\
&c = (B^2E - D^2 - E)(2D_R)^{-1},\\
&d = (BD^2 - B^2F + F){D_R}^{-1},\\
&B = W(\Delta x), \qquad D = W'(\Delta x),\\
&E = W''(0), \qquad F = W''(\Delta x).
\end{aligned} \tag{28}
$$

Equations (28) are obtained by using $\langle R_1R_1\rangle = \langle R_2R_2\rangle = W(0) = 1$, $\langle R_1'R_1'\rangle = \langle R_2'R_2'\rangle = -W''(0)$, $\langle R_1R_2\rangle = W(\Delta x)$, $\langle R_1'R_2'\rangle = -W''(\Delta x)$, $\langle R_1R_1'\rangle = \langle R_2R_2'\rangle = W'(0) = 0$, and $\langle R_1R_2'\rangle = -\langle R_1'R_2\rangle = W'(\Delta x)$, where $\Delta x = x_2 - x_1$, $W(\Delta x) = 2\langle R(0)R(\Delta x)\rangle$, $W'(\Delta x) = \mathrm{d}W/\mathrm{d}\Delta x$, and $W''(\Delta x) = \mathrm{d}^2W/\mathrm{d}(\Delta x)^2$, and, as in Subsection 2.D, for our simulation $W(\Delta x) = 2J_1(\alpha\Delta x)/(\alpha\Delta x)$, with $\alpha = 0.2$.

Carrying out the relatively straightforward, albeit somewhat tedious integrations, we obtain

$$
\begin{aligned}
\Gamma(\Delta x) = &-(\pi^2 n_0)^{-1}[(1 - W^2)W'' + WW'^2]\\
&\times (1 - W^2)^{-3/2} \arcsin(W),
\end{aligned} \tag{29}
$$

where $W = W(\Delta x)$, $W' = W'(\Delta x)$, and $W'' = W''(\Delta x)$. This form for $\Gamma(\Delta x)$ is plotted as $\Gamma(\Delta x/L_{\mathrm{coh}})$ in the solid curve of Fig. 3(a), where it may be seen to be in full agreement with the data. As already indicated, numerical integration of Eq. (29) for this one-dimensional zero-crossing charge correlation function yields $\gamma = 0.9088$, which is the value used in calculating curve a of Fig. 1. In Section 4 we recover the same value for γ from an integration over the two-dimensional vortex charge correlation function $C(\Delta x, \Delta y)$.

3. SCREENING

The average distribution of (topological) charges surrounding some central charge is described by the charge correlation function $C(\Delta\mathbf{r})$.[2] Writing $N_{+/-}(\mathbf{r})$ for the number density of positive/negative charges and defining $N(\mathbf{r}) = N_+(\mathbf{r}) + N_-(\mathbf{r})$, $\Delta N(\mathbf{r}) = N_+(\mathbf{r}) - N_-(\mathbf{r})$, we obtain the equivalent of Eq. (21),

$$
\langle N_+(0)\Delta N(\Delta\mathbf{r})\rangle = \frac{1}{2}\,\eta[\,\delta(\Delta\mathbf{r}) + C(\Delta\mathbf{r})], \tag{30}
$$

where η is the average number density of critical points, the factor of 1/2 arises, as in Subsection 2.F, from $\langle N_+\rangle = \frac{1}{2}\langle N\rangle$, and the Dirac delta function $\delta(\Delta\mathbf{r})$ takes explicit account of the fact that the charge at the origin is perfectly correlated with itself. For a purely random distribution of charges, $C(\Delta\mathbf{r}) = 0$. In the presence of screening, however, $C(\Delta\mathbf{r})$ is mostly negative, and when screening is perfect (i.e., complete),

$$
\int\int_{-\infty}^{\infty} \mathrm{d}^2(\Delta r) C(\Delta\mathbf{r}) = -1. \tag{31}
$$

Below we present measured data for $C(\Delta\mathbf{r})$ for the vortices and for the stationary points (extrema and saddle points) of R and of U, and we compare our data for the vortices with a calculation that is due to Halperin.[2] We also show data for (nontopological) screening of the maxima and the minima of R, as well as for screening of the minima of R and the maxima of I.

As discussed in Section 2, we take the charge of a positive/negative vortex to be its winding number $+/-1$ and the charge of a stationary point to be its topological index, $+1$ for extrema and -1 for saddles. In Fig. 4 we show data measured from our simulation for $2\pi(\Delta r/L_{\mathrm{coh}})C(\Delta r/L_{\mathrm{coh}})$ for (a) the vortices, (b) the stationary points of R, and (c) the stationary points of U. Similar results (not shown) were also measured for the com-

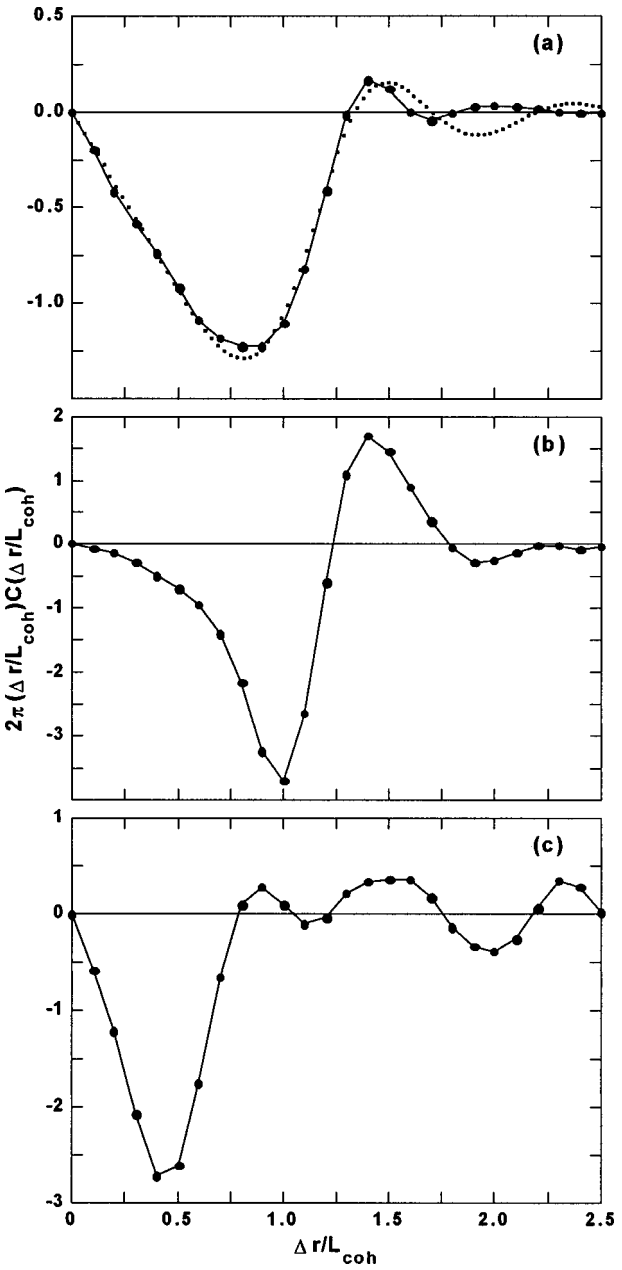

Fig. 4. Critical-point screening. Shown is $2\pi(\Delta r/L_{coh})C(\Delta r/L_{coh})$ versus $\Delta r/L_{coh}$ for (a) the vortices, (b) the real part of the wave function, and (c) the intensity, where the charge correlation function $C(\Delta r)$ is defined in Eq. (30). The solid curves are drawn to aid the eye. The dotted curve in (a) is Eq. (32), a first-principles calculation that is due to Halperin (Ref. 2).

bined critical points of phase (vortices plus stationary points). As the explicit locations of all critical points are required here, the data were obtained from an average over the ten special realizations for which these locations are available. To minimize edge effects, in computing $C(\Delta r)$ we required the central charge to lie at least one coherence length inside the boundary. As may be seen, in each case $C(\Delta r)$ is mostly negative, as expected for screening. Integrating these data numerically, we find that, within the few percent uncertainty of the measurements, Eq. (31) is substantially satisfied over the range of the plots, indicating perfect screening on the scale of a few coherence lengths. We note that randomly permuting the signs of the critical points in Fig. 4 leads in each case to $C(\Delta\mathbf{r}) = 0$, as expected when screening is absent.

The dotted curve in Fig. 4(a) for the vortices is a calculation that is due to Halperin[2]:

$$C(\Delta r) = -\frac{W(0)W'(\Delta r)\{W(\Delta r)[W'(\Delta r)]^2 + W''(\Delta r)[1 - W^2(\Delta r)]\}}{\pi W''(0)\Delta r[1 - W^2(\Delta r)]^2}, \tag{32}$$

where $W'(\Delta r) = dW(\Delta r)/d(\Delta r)$, $W''(\Delta r) = d^2W(\Delta r)/d(\Delta r)^2$, and, once again, for our simulation $W(\Delta r) = 2J_1(\alpha\Delta r)/(\alpha\Delta r)$, with $\alpha = 0.2$. As may be seen, within the uncertainty of the data there is full agreement between our measurements and Halperin's theory.

In Fig. 5 we display $C(\Delta r)$ for (a) screening of the maxima and the minima of R and (b) screening of the minima of R and the maxima of I. [Data for the extrema of I are virtually identical to those in Fig. 5(a) and are not shown.] Here screening is geometrical rather than topological, since the assigned charges are derived not from topological indices but rather from the curvatures of the functions. Accordingly, maxima have a charge of -1, and minima have a charge of $+1$. Worth noting is that these charges are not necessarily conserved and that the

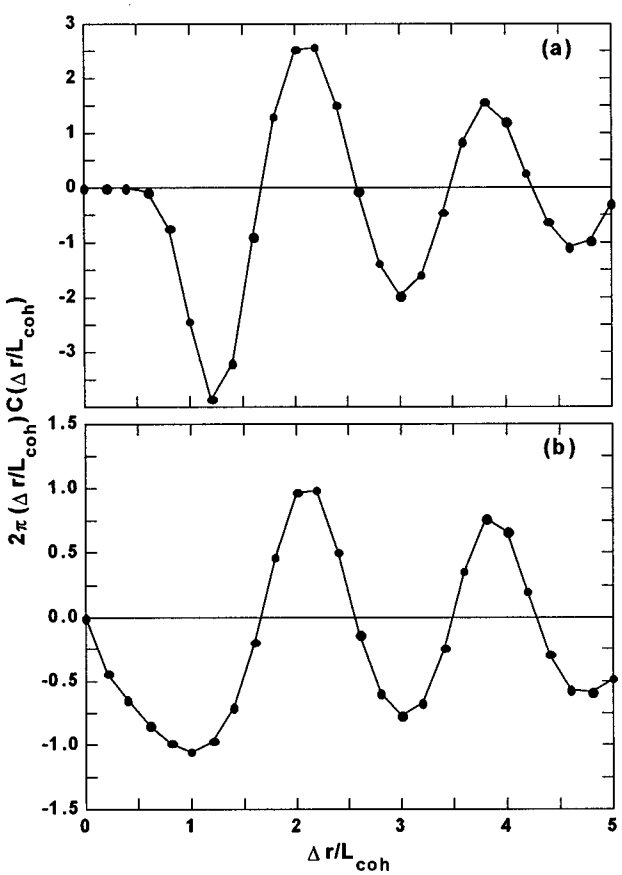

Fig. 5. Screening of extrema. Shown is $2\pi(\Delta r/L_{coh})C(\Delta r/L_{coh})$ versus $\Delta r/L_{coh}$ for (a) all extrema of the real part R of the wave function and (b) minima of R and maxima of the imaginary part I of the wave function. $C(\Delta r)$ is defined in Eq. (30). The solid curves are drawn as aids to the eye.

corresponding charge imbalance cannot be obtained simply from inspection of the boundary. Equation (14) is therefore not applicable, and so there is no *a priori* rationale for screening. Nonetheless, screening is not forbidden, and numerical integration of the data reveals a series of damped oscillations that appear to approach -1 asymptotically, indicating that also here screening may possibly be complete.

The data in Fig. 5(a) for the extrema of R reflect the polycrystalline structure of these critical points,[15,25] which gives rise to the well-defined alternating negative and positive rings surrounding the central charge. These results show that on average the local crystalline structure extends out to a radius of $\sim 5L_{\mathrm{coh}}$. We note that since the number density of extrema is $0.45/L_{\mathrm{coh}}^2$,[24] the wave-field area corresponding to a radius of $5L_{\mathrm{coh}}$ contains some 35 extrema. This surprisingly large number provides a measure of the high degree of local crystallinity that underlies the structure of this supposedly random field.

The data in Fig. 5(b) for mutual screening of real minima and imaginary maxima show the same kind of structure as that in Fig. 5(a). Similar results (not shown) were also found for other combinations of real and imaginary stationary points. This appears paradoxical, since although the real and imaginary parts of the wave function are related by Hilbert transforms, it is well known that these two components of the field are statistically independent.[20] Although the random superposition of two independent perfect lattices with identical lattice constants might be expected to yield results similar to those in Fig. 5(b), it is not at all clear that this should occur for the imperfect, presumably randomly positioned small crystallites that cover approximately half the area of R and I.[15] Randomly permuting the signs of the critical points in Fig. 5 destroys all structure and leads to $C(\Delta\mathbf{r}) = 0$, as expected.

4. SCREENING AND CHARGE FLUCTUATIONS IN A BOUNDED REGION

We now close the circle by developing for a bounded area A an exact relationship between $\langle(\Delta N)^2\rangle$ and the first moment of $C(\mathbf{r})$. Writing

$$\Delta N = \iint_A \mathrm{d}^2 r\ \Delta N(\mathbf{r}) \tag{33}$$

and proceeding as in Subsection 2.F, we have

$$\langle(\Delta N)^2\rangle = 2\int\int_{-\infty}^{\infty} \mathrm{d}^2(\Delta r) A(\Delta\mathbf{r}) \langle N_+(0)\Delta N(\Delta\mathbf{r})\rangle, \tag{34}$$

where

$$A(\Delta\mathbf{r}) = \iint_{-\infty}^{\infty} \mathrm{d}^2 r\ u_A(\mathbf{r}) u_A(\mathbf{r}+\Delta\mathbf{r}), \tag{35}$$

with $u_A(\mathbf{r}) = 1$ inside A and $u_A(\mathbf{r}) = 0$ outside. $A(\Delta\mathbf{r})$ has the usual interpretation as the area of overlap between A and its replica displaced by $\Delta\mathbf{r}$ and for simple shapes is easily computed geometrically. For a rectangular box with sides L_x along x and L_y along y,

$$A(\Delta x, \Delta y) = (L_x - |\Delta x|)(L_y - |\Delta y|) \times H(L_x - |\Delta x|)H(L_y - |\Delta y|), \tag{36}$$

where, as in Subsection 2.F, $H(v) = 1$ for $v \geqslant 0$ and $H(v) = 0$ otherwise. Inserting Eq. (30) into Eq. (34), we obtain the principal result of this section:

$$\langle(\Delta N)^2\rangle = \langle N\rangle + \eta\iint_{-\infty}^{\infty} \mathrm{d}^2(\Delta r) A(\Delta\mathbf{r}) C(\Delta\mathbf{r}), \tag{37}$$

where again η is the average number density of critical points.

We may also express $\langle(\Delta N)^2\rangle$ in terms of the structure factor $S(\mathbf{k})$. Writing

$$C(\Delta\mathbf{r}) = \iint_{-\infty}^{\infty} \mathrm{d}^2 k\ \exp(i\mathbf{k}\cdot\Delta\mathbf{r}) S(\mathbf{k}) \tag{38}$$

and defining

$$\Upsilon(\mathbf{k}) = \iint_{-\infty}^{\infty} \mathrm{d}^2(\Delta r) \exp(i\mathbf{k}\cdot\Delta\mathbf{r}) A(\Delta\mathbf{r}), \tag{39}$$

where $\Upsilon(\mathbf{k})$ has the simple interpretation that it is the far-field Fraunhofer intensity diffraction pattern of an open aperture whose size and shape is that of A,[26] we have

$$\langle(\Delta N)^2\rangle = \langle N\rangle + \eta\iint_{-\infty}^{\infty} \mathrm{d}^2 k \Upsilon(\mathbf{k}) S(\mathbf{k}). \tag{40}$$

For a random collection of charges for which $C(\Delta\mathbf{r}) = 0$, we recover from Eq. (37) the expected result $\langle(\Delta N)^2\rangle = \langle N\rangle$. In the presence of perfect screening, however, we obtain a completely different result. Inserting Eq. (36) into Eq. (37) and assuming (1) Eq. (31) for complete screening within an area small compared with the size of the box and (2) that, for large Δr, $C(\Delta r)$ decays faster than $1/(\Delta r)^3$, we have, to leading order for large boxes,

$$\langle(\Delta N)^2\rangle = \frac{1}{4}\,\eta[\Lambda_s^{(y)} P_x + \Lambda_s^{(x)} P_y], \tag{41}$$

where the anisotropic screening lengths $\Lambda_s^{(x)}$, $\Lambda_s^{(y)}$ are given by

$$\Lambda_s^{(x)} = -2\int_{-\infty}^{\infty} \mathrm{d}(\Delta y) \int_{-\infty}^{\infty} \mathrm{d}(\Delta x) |\Delta x| C(\Delta x, \Delta y), \tag{42a}$$

$$\Lambda_s^{(y)} = -2\int_{-\infty}^{\infty} \mathrm{d}(\Delta y) \int_{-\infty}^{\infty} \mathrm{d}(\Delta x) |\Delta y| C(\Delta x, \Delta y), \tag{42b}$$

and $P_x = 2L_x$, $P_y = 2L_y$. In the isotropic fields of interest here, $\Lambda_s^{(x)} = \Lambda_s^{(y)} = \Lambda_s$. Transforming to polar coordinates Δr and θ and integrating over θ, we obtain

$$\Lambda_s = -8\int_0^{\infty} \mathrm{d}(\Delta r)(\Delta r)^2 C(\Delta r), \tag{43}$$

$$\langle(\Delta N)^2\rangle = \tfrac{1}{4}\,\eta\Lambda_s P. \tag{44}$$

Thus the effect of screening is to cancel the dominant $\langle(\Delta N)^2\rangle = \langle N\rangle = \eta A$ contribution in Eq. (37), leaving a

residual term proportional to the perimeter P. We note that because of the sometimes delicate nature of this cancellation, special care needs to be exercised in the use of approximations. Comparing Eqs. (14) and (44), we obtain the useful connection

$$\gamma = \frac{\eta \Lambda_s}{n_0}. \tag{45}$$

The physical meaning of Eq. (14) now becomes clear. Because of perfect screening, in the interior of A positive and negative charges exactly cancel one another, so that $\langle(\Delta N)^2\rangle$ depends *only* on the unscreened charges that are located near the boundary. The area occupied by these unscreened charges is a strip whose width is of the order of the screening length Λ_s and whose length is the perimeter P. Multiplying this area by the number density η yields the total average number of unscreened charges $\langle N_{\mathrm{unscr}}\rangle$, and since $C(\Delta x, \Delta y) = 0$ for unscreened charges, we recover $\langle(\Delta N)^2\rangle = \langle N_{\mathrm{unscr}}\rangle \sim \eta \Lambda_s P$ from Eq. (37).

Although derived for a rectangular box, it is now apparent from its physical content that Eq. (44), and therefore also Eq. (14), are correct for an arbitrarily shaped area provided that all fingers and fjords have widths and radii of curvature large compared with Λ_s. The results of this section are also easily extended to higher dimensions for any isotropic field containing signed quantities that completely screen one another. Specifically, in k dimensions

$$\Lambda_s = -2 \int \cdots \int_{-\infty}^{\infty} \mathrm{d}^k(\Delta r) |\Delta r_i| C(\Delta \mathbf{r}), \tag{46}$$

where Δr_i is any component of the k-dimensional vector $\Delta \mathbf{r} = (\Delta r_1, \Delta r_2, \ldots, \Delta r_i, \ldots, \Delta r_k)$ and $C(\Delta \mathbf{r})$ is assumed to decay asymptotically faster than $1/(\Delta r)^{k+1}$. In Eq. (44) η is now the number density of signed quantities, and P is the size of the boundary—the length of the perimeter in two dimensions, the area of the surface in three dimensions, etc.

Worth emphasizing is that whenever Eq. (14) is applicable, so is Eq. (31), and the system will exhibit perfect screening. The converse is not necessarily true, however, and quantities that cannot be counted by means of a boundary walk can still exhibit mutual screening. This is illustrated by the data for extrema in Fig. 5. Equation (37) holds in all cases, however, as does Eq. (44) when Eq. (31) is applicable, so these results are of greater generality than is Eq. (14).

We can quantitatively test the results of this section by using Halperin's form for $C(\Delta r)$ for the vortices.[2] We first obtain Λ_s by inserting Eq. (32) into Eq. (43) and carry out the required integration numerically. Then, using this value for Λ_s together with the known exact values for η and n_0 in Eq. (45), we recover $\gamma = 0.9088$, in complete accord with the value obtained from Eqs. (23) and (29). We recall that this value of γ is in full accord with the data for $\langle(\Delta N)^2\rangle$ in curve a of Fig. 1.

We also test Eq. (37) for small boxes by again using Halperin's form for $C(\Delta r)$ for the vortices. In Fig. 6(a) we show a comparison between theory and measurement for values of the perimeter P between L_{coh} and $12L_{\mathrm{coh}}$. For boxes whose sizes are less than the screening length, we have $\langle(\Delta N)^2\rangle \sim N \propto P^2$, and in this region $\langle(\Delta N)^2\rangle$ is always less than the linear asymptotic prediction in Eq. (14). In light of the small difference of 0.13 between the asymptotic and exact forms for $\langle(\Delta N)^2\rangle$ together with an uncertainty of ± 0.05 in the data, the degree of quantitative agreement between the exact theory and the measurements appears reasonable, and so this agreement adds additional support to the theory of Eq. (37). In Fig. 6(b) we plot the calculated percentage difference between the asymptotic form in Eq. (14) and the exact form in Eq. (37). As may be seen, this difference falls relatively slowly as L_{coh}^{-1}, dropping below 1% only at $P \approx 66 L_{\mathrm{coh}}$.

Even if $C(\Delta r)$ is not known, the screening length Λ_s can still be obtained from Eq. (45) if γ, η, and n_0 are available. Illustrating this procedure for the vortices (for which, of course, all parameters including Λ_s are known), we have γ from Eqs. (23) and (29), $\eta = (2\pi)^{-1} \times [-W^{(2)}(0)/W(0)]$, as given by Berry,[8] Baranova *et al.*,[27] and Halperin,[2] and $n_0 = \pi^{-1}[-W^{(2)}(0)/W(0)]^{1/2}$ from Rice,[22] where $W^{(n)}(\Delta r) = \mathrm{d}^n W(\Delta r)/[\mathrm{d}(\Delta r)]^n$. This yields $\Lambda_s = 2\gamma[-W(0)/W^{(2)}(0)]^{1/2}$. Inserting numerical values appropriate to our simulation, we obtain $\Lambda_s = 0.949 L_{\mathrm{coh}}$.

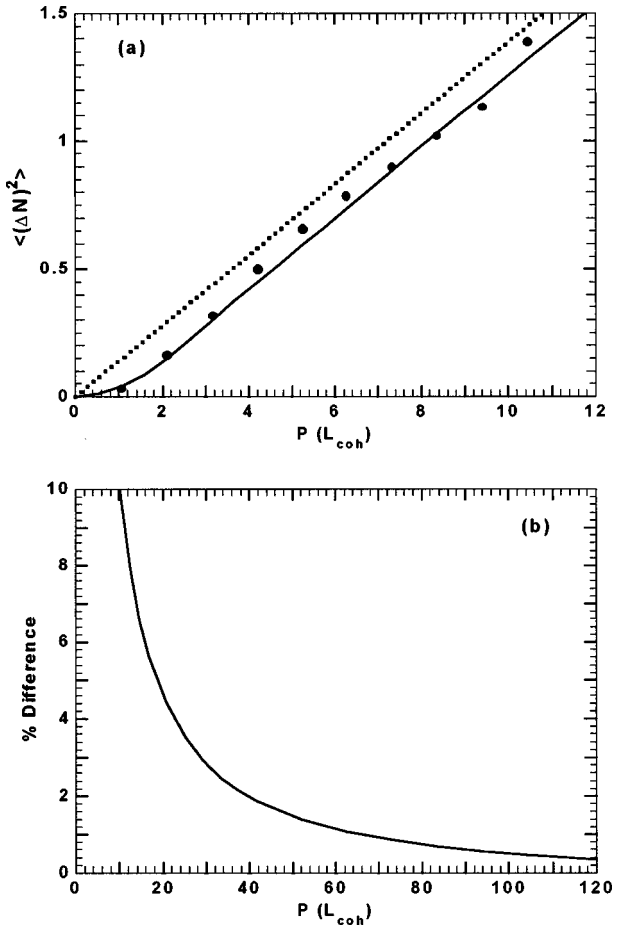

Fig. 6. Variance $\langle(\Delta N)^2\rangle$ of topological charge imbalance for small square boxes with perimeter P: (a) the filled circles are measured data, the solid curve is the exact form in Eq. (37), and the dotted curve is the asymptotic form in Eq. (14); (b) percent difference between the asymptotic and exact forms.

For the stationary points of R, for which $C(\Delta r)$ is not known analytically, we have $\gamma = 0.72$ from the data of Subsection 2.D. From Longuet-Higgins[24] we have $\eta = 2(3\sqrt{3}\pi)^{-1}[-W^{(4)}(0)/W^{(2)}(0)]$, and from Ref. 21 we have $n_0 = \pi^{-1}[-W^{(4)}(0)/W^{(2)}(0)]^{1/2}$. This yields $\Lambda_s = (3\sqrt{3}\gamma/2)[-W^{(2)}(0)/W^{(4)}(0)]^{1/2} = 0.69L_{\mathrm{coh}}$ for our simulation.

For the stationary points of U, for which again $C(\Delta r)$ is not known analytically, we have $\gamma = 1.12$ from the data of Subsection 2.D, $\eta = 2(0.337)[-W^{(2)}(0)/W(0)]$ from Weinberg and Halperin,[28] and, to sufficient accuracy, $n_0 \cong \pi^{-1}[-W^{(2)}(0)/W(0)]^{1/2}[2(1 + \beta/8)]$ and $\beta = -1 + W(0)W^{(4)}(0)/[-W^{(2)}(0)]^2$ from Ref. 21. Inserting numerical values appropriate to our simulation, we obtain $\Lambda_s = 0.62L_{\mathrm{coh}}$.

For the combined critical points of phase, we have from Subsection 2.D the estimate $\gamma = 1.0$. We also have $\eta = [\pi(1 - \epsilon)]^{-1}[-W^{(2)}(0)/W(0)]$ from a recent sum rule for these critical points[14] and $n_0 = (\beta/\pi)[-W^{(2)}(0)/W(0)]^{1/2}$ from Ref. 21. Here ϵ arises from the relatively small number of extrema present in the phase field, which consists principally of phase saddles strung between vortices. For our simulation $\epsilon \simeq 1/14$, and so $\Lambda_s = 0.5L_{\mathrm{coh}}$.

We note that these values for Λ_s are less than the apparent range of $C(\Delta r)$ in Figs. 4 and 5. This occurs because a given (say) positive charge is typically surrounded by alternating rings of negative and positive charges, with the first negative ring tending to overscreen, so that complete charge cancellation requires only part of this first ring.

5. SUMMARY

Topological charge fluctuations and critical-point screening in a bounded region have been discussed for the vortices, as well as for the critical points of the real part of the wave function, the intensity, and the phase. In all cases the critical points of these fields are found to screen one another completely. The critical points of the statistically independent real and imaginary parts of the wave function have also been found to screen one another, demonstrating the ubiquitous nature of screening. It was shown that because of this screening, charges in the interior of the region cancel one another, so that the net charge imbalance and its fluctuations are due only to unscreened charges near the boundary. It was also shown that the charge imbalance of all critical points within a bounded region can be determined from a count of signed zero crossings on the boundary. This result opened a highly convenient route for both measurement and calculation of the charge imbalance and its variance. A first-principles calculation for isotropic Gaussian fields was given for the variance of the vortex charge imbalance and shown to be in full agreement with data from large-scale computer simulations. An exact relationship between the charge correlation function and the variance in a bounded region was derived, and this too was verified by comparison with the data.

ACKNOWLEDGMENTS

M. Wilkinson thanks the Physics Department at Bar-Ilan University for its hospitality during a visit when part of this work was done and is also pleased to acknowledge support by the Engineering and Physical Sciences Research Council (UK) (grant GR/L/02302). I. Freund acknowledges a number of highly useful discussions with David A. Kessler, as well as support of the Israel Science Foundation of the Israel Academy of Arts and Sciences.

I. Freund's e-mail address is freund@mail.biu.ac.il; M. Wilkinson's e-mail address is cabs12@ccsun.strath.ac.uk.

REFERENCES

1. B. W. Roberts, E. Bodenschatz, and J. P. Sethna, "A bound on the decay of defect–defect correlation functions in two-dimensional complex order parameter equations," Physica D **99**, 252–268 (1996).
2. B. I. Halperin, "Statistical mechanics of topological defects," in *Physics of Defects*, R. Balian, M. Kleman, and J.-P. Poirier, eds. (North-Holland, Amsterdam, 1981), pp. 814–857.
3. J. M. Kosterlitz and D. J. Thouless, "Two-dimensional physics," in *Progress in Low Temperature Physics*, B. D. F. Brewer, ed. (North-Holland, Amsterdam, 1978), Vol. VIIB, pp. 371–433.
4. D. J. Thouless, M. Kohmoto, M. P. Nightingale, and M. den Nijs, "Quantized Hall conductance in a two-dimensional periodic potential," Phys. Rev. Lett. **49**, 405–408 (1982).
5. P. N. Walker and M. Wilkinson, "Universal fluctuations of Chern integers," Phys. Rev. Lett. **74**, 4055–4058 (1995).
6. J. F. Nye and M. V. Berry, "Dislocations in wave trains," Proc. R. Soc. London, Ser. A **336**, 165–190 (1974).
7. M. Berry, "Singularities in waves and rays," in *Physics of Defects*, R. Balian, M. Kleman, and J.-P. Poirier, eds. (North-Holland, Amsterdam, 1981), pp. 453–549.
8. M. Berry, "Disruption of wave-fronts: statistics of dislocations in incoherent Gaussian random waves," J. Phys. A **11**, 27–37 (1978).
9. V. I. Arnold, *Ordinary Differential Equations* (MIT Press, Cambridge, Mass., 1973), Chap. 5, pp. 254–268.
10. S. H. Strogatz, *Nonlinear Dynamics and Chaos* (Addison-Wesley, Reading, Mass., 1994).
11. N. Shvartsman and I. Freund, "Vortices in random wave fields: nearest neighbor anticorrelations," Phys. Rev. Lett. **72**, 1008–1011 (1994).
12. I. Freund and N. Shvartsman, "Wave-field phase singularities: the sign principle," Phys. Rev. A **50**, 5164–5172 (1994).
13. I. Freund, "Amplitude topological singularities in random electromagnetic wavefields," Phys. Lett. A **198**, 139–144 (1994).
14. I. Freund, "Saddles, singularities, and extrema in random phase fields," Phys. Rev. E **52**, 2348–2360 (1995).
15. I. Freund, "'1001' correlations in random wave fields," Waves Random Media **8**, 119–158 (1998).
16. I. Freund, "Vortex derivatives," Opt. Commun. **137**, 118–126 (1997).
17. R. Loudon, *The Quantum Theory of Light* (Oxford U. Press, Oxford, 1983), Chap. 6, pp. 226–229.
18. I. Freund, "Optical vortices in Gaussian random wave fields: statistical probability densities," J. Opt. Soc. Am. A **11**, 1644–1652 (1994).
19. I. Freund and D. A. Kessler, "Phase autocorrelation of random wave fields," Opt. Commun. **124**, 321–332 (1996).
20. J. W. Goodman, *Statistical Optics* (Wiley, New York, 1985), Chap. 5, pp. 207–222.
21. D. A. Kessler and I. Freund, "Level-crossing densities in random wave fields," J. Opt. Soc. Am. A **15**, 1608–1618 (1998).
22. S. O. Rice, "Mathematical analysis of random noise," in *Se-*

lected Papers on Noise and Stochastic Processes, N. Wax, ed. (Dover, New York, 1954), pp. 133–294.
23. S. O. Rice, "Distribution of the duration of fades in radio transmission," Bell Syst. Tech. J. **37**, 581–635 (1958).
24. M. S. Longuet-Higgins, "The statistical analysis of a random moving surface," Philos. Trans. R. Soc. London, Ser. A **249**, 321–387 (1957).
25. I. Freund and N. Shvartsman, "Structural correlations in Gaussian random wave fields," Phys. Rev. E **51**, 3770–3773 (1995).
26. J. W. Goodman, *Introduction to Fourier Optics*, 2nd ed. (McGraw-Hill, San Francisco, 1988), Chap. 4, pp. 73–83.
27. N. B. Baranova, B. Y. Zel'dovich, A. V. Mamaev, N. Pilipetskii, and V. V. Shkukov, "Dislocations of the wave-front of a speckle-inhomogeneous field (theory and experiment)," JETP Lett. **33**, 195–199 (1981).
28. A. Weinberg and B. I. Halperin, "Distribution of maxima, minima, and saddle points of the intensity of laser speckle patterns," Phys. Rev. B **26**, 1362–1368 (1982).